The crystal structure of the light-harvesting complex II (B800–850) from *Rhodospirillum molischianum*

Juergen Koepke[1], Xiche Hu[2], Cornelia Muenke[1], Klaus Schulten[2]* and Hartmut Michel[1]*

Background: The light-harvesting complexes II (LH-2s) are integral membrane proteins that form ring-like structures, oligomers of αβ-heterodimers, in the photosynthetic membranes of purple bacteria. They contain a large number of chromophores organized optimally for light absorption and rapid light energy migration. Recently, the structure of the nonameric LH-2 of *Rhodopseudomonas acidophila* has been determined; we report here the crystal structure of the octameric LH-2 from *Rhodospirillum molischianum*. The unveiling of similarities and differences in the architecture of these proteins may provide valuable insight into the efficient energy transfer mechanisms of bacterial photosynthesis.

Results: The crystal structure of LH-2 from *Rs. molischianum* has been determined by molecular replacement at 2.4 Å resolution using X-ray diffraction. The crystal structure displays two concentric cylinders of sixteen membrane-spanning helical subunits, containing two rings of bacteriochlorophyll-a (BChl-a) molecules. One ring comprises sixteen B850 BChl-as perpendicular to the membrane plane and the other eight B800 BChl-as that are nearly parallel to the membrane plane; eight membrane-spanning lycopenes (the major carotenoid in this complex) stretch out between the B800 and B850 BChl-as. The B800 BChl-as to exhibit a different ligation from that of *Rps. acidophila* (aspartate is the Mg ligand as opposed to formyl-methionine in *Rps. acidophila*).

Conclusions: The light-harvesting complexes from different bacteria assume various ring sizes. In LH-2 of *Rs. molischianum*, the Q_y transition dipole moments of neighboring B850 and B800 BChl-as are nearly parallel to each other, that is, they are optimally aligned for Förster exciton transfer. Dexter energy transfer between these chlorophylls is also possible through interactions mediated by lycopenes and B850 BChl-a phytyl tails; the B800 BChl-a and one of the two B850 BChl-as associated with each heterodimeric unit are in van der Waals distance to a lycopene, such that singlet and triplet energy transfer between lycopene and the BChl-as can occur by the Dexter mechanism. The ring structure of the B850 BChl-as is optimal for light energy transfer in that it samples all spatial absorption and emission characteristics and places all oscillator strength into energetically low lying, thermally accessible exciton states.

Introduction

Photosynthetic purple bacteria possess up to three light harvesting (antenna) complexes (LHs) besides the reaction center, and these are integrated into the membrane. The peripheral antenna complexes, LH-2 and LH-3, have absorption maxima at shorter wavelengths than the core antenna complex, LH-1, and the reaction center itself; the latter usually absorbs at the lowest energy and utilizes the collected light energy for photoinduced electron transfer, which fuels cellular processes. The antenna complexes broaden the spectral region of the light which can be used by the bacterium. Energy is transferred efficiently from one complex to another and finally to the reaction center.

The LHs from purple bacteria are oligomers. The basic unit is a heterodimer consisting of two small protein sub-units often referred to as α- and β-apoproteins. The αβ-heterodimers of LH-2 and LH-3 bind three bacterio-chlorophyll-a (BChl-a) molecules. Due to the different molecular surroundings of these BChl-as, one absorbs maximally at around 800 nm while the other two show maximal absorption at around 850 and 820 nm in LH-2 and LH-3, respectively [1]. Hence, a first energy transfer can already take place between BChl-as inside LH-2 or LH-3 from those absorbing at shorter to those absorbing at the longer wavelength. Between the long wavelength bands of LH-3 (820 nm) and LH-2 (850 nm) energy transfer is possible. Because the BChl-as of LH-1

absorb around 880 nm [2], energy can also be transferred from the long wavelength bands of LH-2 or LH-3 to the LH-1 BChl-as. LH-1 is believed to form a ring around the reaction center [3].

The LH-2 of *Rhodospirillum molischianum* exhibits two absorption maxima, at 800 and 846 nm, and is often referred to as the B800–850 complex. The B800 and B850 BChl-as of LH-2 are not in direct van der Waals contact, and neither are the B850 BChl-a of LH-2 and the B880 BChl-a of LH-1. The BChl-as can transmit energy through two possible mechanisms, the Förster mechanism [4] and the Dexter mechanism [5]. The Förster mechanism can operate over a long distance (~20 Å) and is most efficient when the BChl-a Q_y transition dipole moments are co-linear or at least parallel [6]. The Dexter mechanism [5] requires overlap of wave functions in order to be effective, that is, it is necessary for partners to be in close contact. Thus, detailed information on the spatial arrangement of chromophores is crucial to understand the mechanism of energy transfer in the photosynthetic membrane.

Two-dimensional (2D), or preferably 3D, crystals are necessary to obtain information about the structure of membrane proteins. LH-2 complexes from several bacteria have been crystallized in 3D [7–11] and 2D crystals have been obtained for LH-1 complexes [12]. Although the structures of the bacterial reaction centers [13–17] have been known for nearly a decade, the structure of a plant light harvesting complex (LHC II) has been determined only recently, by electron crystallography [18]. The plant LHs show no structural similarities to the bacterial LHs. A projection map of the bacterial LH-1 from *Rhodospirillum rubrum* is available at 8.5 Å resolution [3] and of the LH-2 from *Rhodovulum sulfidophilum* at 18 Å resolution [19]. Most recently, the structure of the bacterial LH-2 of *Rhodopseudomonas acidophila* [20], determined by X-ray crystallography to 2.5 Å resolution, allowed one to take a closer look at bacterial LHs. The investigations revealed ring-shaped arrangements, which have different sizes in the various bacteria, for both LH-1 and LH-2. The αβ-heterodimeric building unit consists of the α- and β-apoproteins, the BChl-a molecules, and carotenoids, and is repeated nine times in the LH-2 from *Rps. acidophila*. The LH-1 from *Rs. rubrum* forms a ring with a 16-fold axis and an interior large enough to accommodate a reaction-center complex [3].

LH-2 of *Rs. molischianum*, investigated here, has marginal sequence homology [21] to LH-2 of *Rps. acidophila* (26% and 31% overall identity for the α- and the β-subunit, respectively). For the majority of the LH-2 and LH-1 complexes there exists a methionine at the N terminus of the α-apoprotein and this residue can bind the B800 BChl-a [20,22]. However, the N-terminal residue of the α-apoprotein of *Rs. molischianum* is a serine and therefore a different method of binding the B800 BChl-a is required. A further difference between LH-2s from *Rs. molischianum* and *Rps. acidophila* lies in the size of the oligomer. Whereas LH-2 of *Rps. acidophila* is a nonamer of αβ-heterodimers, analytical ultracentrifugation [23] and SDS-PAGE have yielded a molecular weight of about 100 kDa for the native pigment–protein complex of LH-2 from *Rs. molischianum;* this weight agrees with an octameric ($α_8β_8$) structure, which is also in agreement with electron micrographs [24].

In the following, we describe the determination of the structure of LH-2 of *Rs. molischianum* to 2.4 Å resolution by the molecular replacement method. The procedure for building a computationally modelled search model is presented, including structure prediction, homology modelling and molecular dynamics. We introduce a molecular replacement approach that can be used for placing multiple proteins into the unit cell in the event of close crystal packing. The resulting structure of LH-2 of *Rs. molischianum* is characterized and discussed in view of the biological function of the protein. In particular, the geometry of the chromophore arrangement is related to the internal and external light energy transfer processes occurring in LH-2.

Results
Structure solution using molecular replacement
Tetragonal crystals of LH-2 from *Rs. molischianum* have been obtained that belong to the space group $P42_12$ with cell dimensions a=b=91.6 Å, c=210.0 Å. X-ray diffraction data have been collected up to 2.4 Å resolution. Upon variation of the crystallization conditions more than a dozen crystal forms have been obtained, but only crystals of the tetragonal form described diffracted X-rays to high resolution. Handling of these crystals was a considerable problem, as the mother liquor had to be supersaturated with heptane-1,2,3-triol (HPTO) to prevent the crystals redissolving. Upon long term storage or manipulation of the crystals, HPTO frequently crystallizes and the concentration of HPTO in solution decreases. As the size of the detergent micelle depends inversely on the HPTO concentration [25,26], the detergent micelle increases in size and can no longer be accommodated in the protein's crystal lattice. As a result, the crystals often crack and the protein redissolves [11].

The relevant tetragonal crystal form of LH-2 was originally discovered with dodecylamine-N,N-dimethyl-N-oxide (LDAO) as detergent, but could be reproduced only in about 30% of the crystallization trials. By using undecylamine-N,N-dimethyl-N-oxide (UDAO), the reproducibility was increased to 100%, whereas with decylamine-N,N-dimethyl-N-oxide this crystal form was rarely observed. Due to the need to supersaturate the mother liquor with HPTO, it was not possible to use classical

soaking experiments to search for heavy atom derivatives. Cocrystallization was tried as an alternative, but no derivatives could be identified. Therefore, the 3D structure of LH-2 from *Rs. molischianum* was determined by the molecular replacement method, using a computationally modelled octamer of the αβ-heterodimers as a search model. The αβ-heterodimer was built using homology modelling that was based on the 2.5 Å resolution crystal structure of LH-2 of *Rps. acidophila* [20].

Orientations and positions of the LH-2 complexes in the unit cell were determined by a direct search, which was conducted in limited degrees of freedom with constraints derived from conventional rotational and translational searches, as detailed below. The complex possesses an eightfold non-crystallographic symmetry (NCS), the axis coinciding with the crystallographic fourfold rotational axis. Each asymmetric unit contains two motifs, each motif belonging to a crystallographically independent octameric complex. The two octamers are centered at fractional coordinates of (0, 0.5, 0.139) and (0, 0.5, 0.365); they are oriented parallel and antiparallel to the z-axis, respectively. As each motif consists of two heterodimers, there are a total of four heterodimers within the asymmetric unit, and these are related by four NCS operations.

The current model for each heterodimer includes 99 residues, 56 from the β-apoprotein and 43 from the β-apoprotein, three BChl-a molecules, and one lycopene (the major carotenoid of the complex). A total of 16 water molecules, three UDAO and six HPTO molecules were placed per αβ-heterodimer.

Assessment of structural quality

A Ramachandran plot (not shown) of the current model indicates that 95.4% of the residues fall in the most favoured regions and only 4.6% are found in the additionally allowed regions. Both apoproteins are preferentially in an α-helical conformation, due to their long membrane spanning α helices. The α-apoprotein forms two smaller additional helices close to its N and C termini. The C-terminal helix is also α helical, whereas that at the N terminus is a 3_{10} helix according to the criteria of Kabsch and Sander [27].

Computation of the real space correlation coefficient [28] for all residues, determined with all atoms, of the calculated model electron density $2F_o–F_c$ map showed that the correlation of the membrane-spanning helices and the C-terminal helix of the α-apoprotein was very good (~90%). However, the correlation of the N terminus of the β-apoprotein was not of the same quality. We were not able to find a useful density for the first two residues of the β-apoprotein.

The average B-values for main-chain and side-chain atoms only show high temperature factors of the terminal regions of the two apoproteins. All other residues have B-factors close to $B_{Wilson}=47$ Å^2 (an estimate of the average temperature factor for the crystal). The N terminus of the β-apoprotein and, to a lesser extent, the N terminus of the α-apoprotein exhibit very large B-factors. As the number of contacts to neighbouring and symmetry related octamers is a lot less on the N-terminal side of the octamer, it seems likely that the N termini of the two apoproteins exhibit high flexibility. The lower temperature factors for N-terminal residues of the α-apoprotein probably reflect the involvement of these residues in binding the B800 BChl-a.

The electron density is continuous along the apoprotein chains, except for the first three residues of the β-apoprotein. Also, the lycopene and the two B850 BChl-as are well defined, as demonstrated in Figure 1. Only the phytyl chain of the B800 BChl-a is less well defined; the density that could be fitted to this phytyl tail shows a large gap beyond the ninth carbon atom; we omitted all further atoms of this tail.

Figure 1

Stereo pair of the electron density around the pigment molecules, providing an example of the quality of the $2F_o–F_c$ map at a contouring level of 1σ.
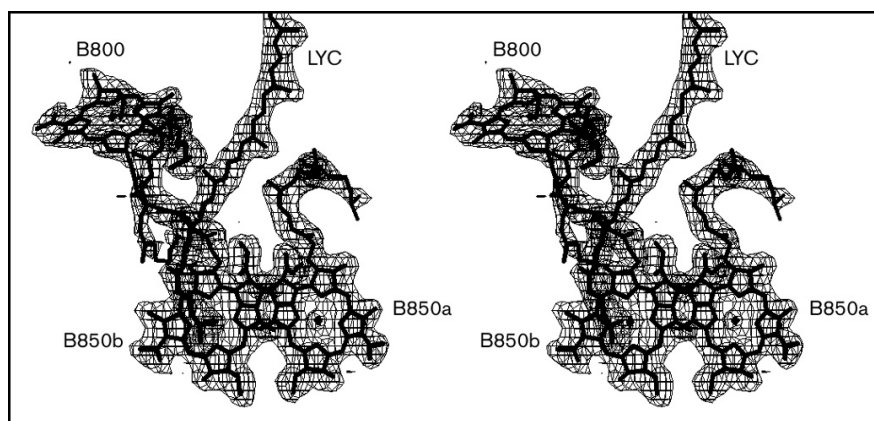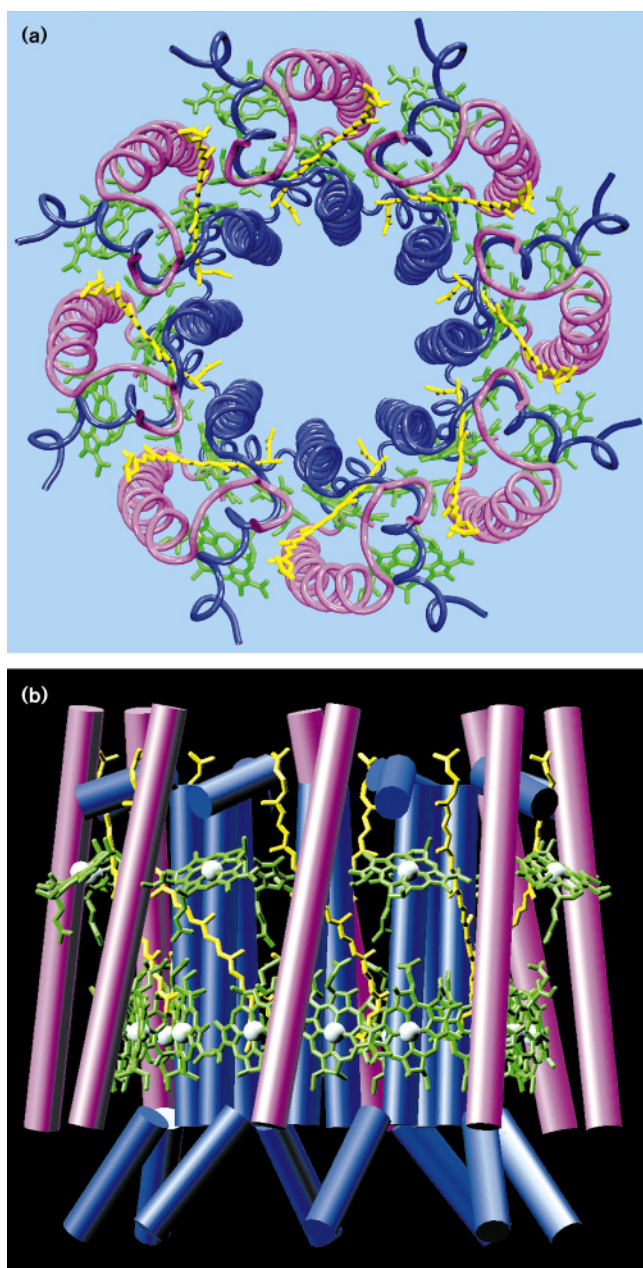
Figure 2

The LH-2 octameric complex from *Rs. molischianum*. (a) View from above with N termini pointing upward. The apoproteins are represented as Cα tracing tubes with the α-apoproteins (inside) in blue and the β-apoproteins (outside) in magenta. The bacteriochlorophyll-a molecules are in green with their phytyl tails truncated for clarity. The lycopenes are in yellow. (b) Side view, using the same colors as in (a), with the α-helical segments represented as cylinders and the Mg atoms as white spheres. (Figure was produced with the program VMD [62,63], and then rendered with Rayshade.)

A Luzzati plot [29] indicates that the error in the coordinate positions, calculated using X-PLOR [30] with the test dataset for calculations of the free R-value [31,32] (23.2%), lies between 0.3 and 0.35 Å. When the work dataset is used (R-value=21.1%), the coordinate error seems to be slightly better (by 0.05 Å) only for reflections with low resolution (>3.5 Å) [33,34].

Overall structure

The crystal structure of LH-2 from *Rs. molischianum* is presented in its entirety in Figure 2. The structure shows an αβ-octamer shaped as a hollow cylinder of 90 Å diameter, formed by the membrane spanning helices of the two apoproteins, with the α-apoprotein inside and the β-apoprotein outside. The diameter of the inner helical ring is 31 Å, as measured between the central axes of the helices, and that of the outer helical ring measures 62 Å. The height of the cylinder is 50 Å.

The α- and β-apoproteins can be considered as the building blocks that make up the smallest repeating unit, the αβ-heterodimer. A stereo diagram of the αβ-heterodimer is shown in Figure 3. This heterodimer is repeated eight times around the crystallographic fourfold axis. The membrane-spanning α helix of the β-apoprotein consists of 34 residues (β-Thr9 to β-Lys42). It is tilted against the z-axis by about 10° and is slightly bent on its N-terminal side. The membrane-spanning helix of the α-apoprotein is a straight α helix of 27 residues (α-Asn14 to α-Ala40), oriented perpendicularly, to within 2°, to the membrane (see also Fig. 2). The C-terminal α helix (α-Asn44 to α-Lys56) is amphiphilic with charged and highly polar residues (α-Lys52, α-Lys56) fully exposed to the extra-membranous medium. This α helix is tilted slightly away from the surface of the membrane (see Fig. 3). The amphiphilic N-terminal 3_{10} helix (α-Pro3 to α-Ile13) is located in the membrane–water interface, diving into the membrane to bind the B800 BChl-a; the nonpolar residues Ile9 and Ile13, as well as Asp6 bound to the central Mg of B800 BChl-a, point into the membrane; the charged residues Lys4, Asp5, and Lys8 point away from the membrane. It is worth mentioning that a 'salt bridge' between β-Asp18 and β-Lys21, both located in the interior of membrane, was found. However, it is more likely that in the low dielectric environment of the membrane both residues are neutral and hydrogen bonded. To simplify the following discussion, we will denote by B850a the B850 BChl-a binding to the α-apoprotein, and by B850b the B850 BChl-a binding to the β-apoprotein (see Fig. 3).

As shown in Figure 4, sixteen B850 BChl-a molecules form a ring with each BChl-a oriented perpendicular to the plane of the membrane and sandwiched between the helical apoproteins. The Mg to Mg distance between neighboring B850 BChl-as is 9.2 Å within the αβ-heterodimer and 8.9 Å between the heterodimers; it should be noted that the latter distance is shorter.

The B800 BChl-as form another ring of eight bacteriochlorophylls, also presented in Figure 4, with a Mg to Mg

Figure 3

Stereo drawing of the LH-2 αβ-heterodimer from *Rs. molischianum*: cyan, α-apoprotein; magenta, β-apoprotein; green, BChl-as; yellow, lycopene. (Figure was produced with the program VMD [62].)
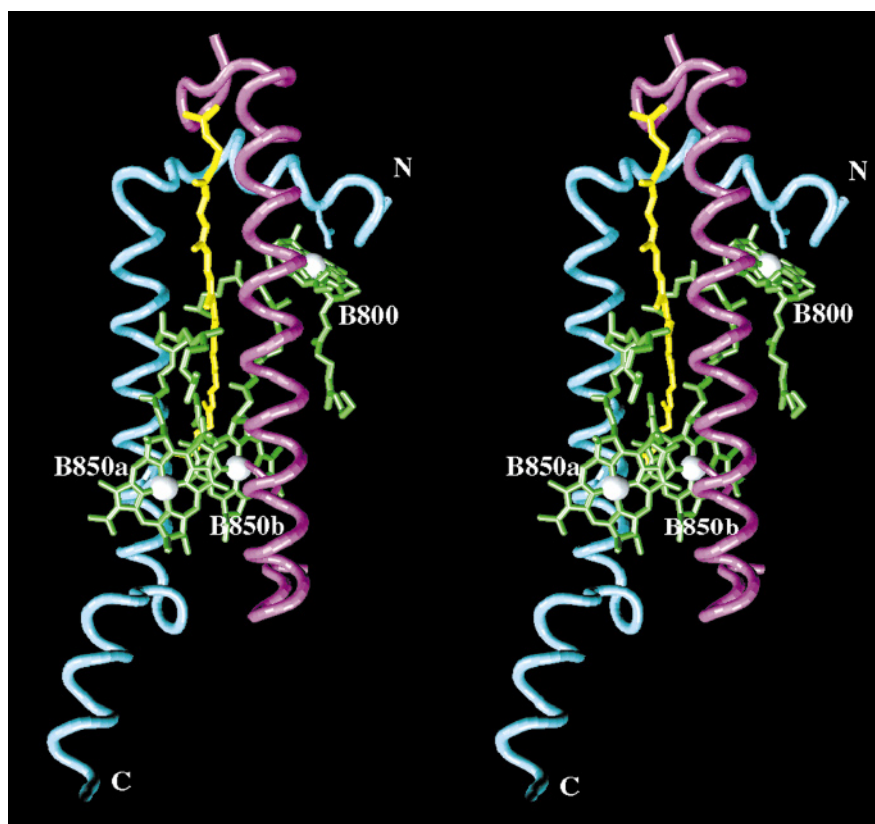
separation of 22.0 Å between neighboring BChl-as. The B800 BChl-as are located between the β-apoproteins and are held in place by the 3_{10} helix of the α-apoproteins. The planes of the B800 BChl-as are tilted away from the membrane plane by 38°.

Interactions governing the oligomerization of apoproteins

The interactions between the α- and β-apoproteins that lead to formation of the octameric LH-2 are governed by indirect interactions through the chlorophylls as well as direct interactions near the water–membrane interface. The Nε2 atoms of α-His34 and β-His35 form ligands to the central Mg atoms of the B850 BChl-as which are completely buried inside the membrane; adjacent B850 BChl-as are in van der Waals contact thereby stabilizing the individual αβ-heterodimers as well as their aggregation. The angle between planes of neighboring B850s is 167.5° within the αβ-heterodimer and 147.5° between the heterodimers. The angle values can be written as 157.5°±10°; 157.5° would be the angle enclosing neighboring edges in a regular 16-sided polygon corresponding to an octameric LH-2. One might speculate that local steric interactions could control the specific angles and, thereby, control the ring size of the LH. For example, in case of LH-2 of *Rps. acidophila* local interactions might prefer angles at 160°±δ

which would be the angle for a regular 18-sided polygon, with δ being the local deviation, and thereby induce a nonamer conformation.

Direct interactions supporting the oligomerization of apoproteins in LH-2 are furnished by hydrogen-bond contacts. Between the two apoproteins belonging to the same αβ-heterodimer, hydrogen bonds can be identified between the N-terminal 3_{10}-helix of the α-apoprotein and the N-terminal residues of the β-apoprotein: β-Ser6 Oγ to α-Trp10 O (2.50 Å); β-Ser6 N to α-Leu11 O (2.75 Å); β-Leu5 N to α-Leu11 O (3.08 Å); β-Glu10 Oε2 to α-Tyr7 Oη (2.83 Å); and β-His17 Nδ1 to α-Trp10 Nε1 (3.12 Å). Hydrogen-bond interactions between the α- and β-subunits of neighboring αβ-heterodimers are α-Asn2 Nδ2 to β′-Gln19 Oδ1 (3.16 Å); α-Asn2 Oδ1 to β′-Gln19 Nε2 (3.12 Å); and α-Ser53 Oγ to β′-Pro43 O (3.53 Å). β′ denotes, here and below, β-apoproteins from a neighboring αβ-heterodimer. We will adopt an analogous notion for any other components of neighboring αβ-heterodimers hereafter. The α-helical segment at the C terminus of the α-apoprotein facilitates the oligomerization through van der Waals interactions with the C-terminal residues of the β-apoproteins of the same αβ-heterodimer and the neighboring αβ-heterodimer.

Figure 4
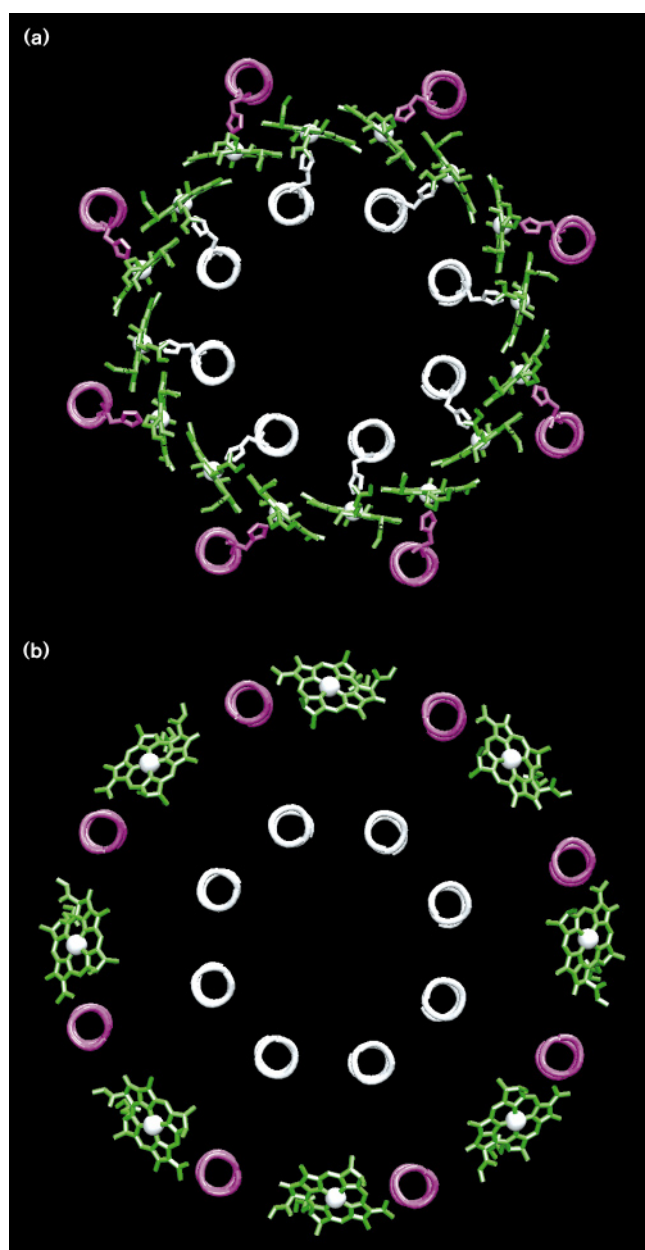
Arrangement of bacteriochlorophylls in the LH-2 of *Rs. molischianum*. (a) View from above the membrane showing the ring of sixteen B850 BChl-as (green) sandwiched between transmembrane helices of the α- and β-apoproteins (white and magenta, respectively). (b) Ring of eight B800 BChl-as (green): the Mg to Mg separation between neighboring B800s is 22.0 Å. Both views are rendered with the same coordinate transformation. (Figure was produced with the program VMD [62].)

Bacteriochlorophyll B850 binding

The binding site for B850 BChl-as is shown in Figure 5a. Two conserved histidines (α-His34 and β-His35) are the ligands of the central Mg atoms of the BChl-as. The distances between the Mg atoms and the Nε2 atoms are 2.27 Å (α-His34) and 2.32 Å (β-His35). Two tryptophans (α-Trp45 and β-Trp44) are within hydrogen-bond distances of the 2-acetyl carbonyl oxygen atoms (O6; we use the old Fischer nomenclature for the bacteriochlorophylls, as the oxygen atoms — in contrast to the new IUPAC system — are individually numbered) of the two BChl-a molecules. The distance from the O6s to Nε1 of α-Trp45 is 2.88 Å; it is possible that Nε1 of β-Trp44 forms an even stronger hydrogen bond, as it is only 2.79 Å from the O6s. A more important role for β-Trp44 is also suggested by the fact that this residue is conserved in all LHs of photosynthetic bacteria, whereas α-Trp45 is not. The binding environment of the B850 BChl-as is non-polar. In addition to the BChl-a binding ligands α-His34 and β-His35, six further aromatic residues (α-Phe43, α-Trp45, β-Trp39, β-Trp41, β-Trp44, β-Phe45) cluster around the B850 BChl-a, near the periplasmic membrane–water interface. The 9-keto groups of either B850 BChl-a do not seem to be involved in hydrogen bonding, which is at variance with conclusions drawn from resonance Raman data [21].

Bacteriochlorophyll B800 binding

Usually the Mg atoms of chlorophyll molecules are liganded by histidine residues. However, in LH-2 of *Rps. acidophila* the ligand of B800 BChl-a is a formyl-methionine. In principle, peptide oxygens, acidic amino acid side chains (aspartate, glutamate), their amides (asparagine, glutamine), serine, threonine, histidine, methionine or even water can interact with the central Mg atom of BChl-a [35]. In fact, in the BChl–protein complex from *Prosthecochloris aestuarii* the Mg of BChl 2 is coordinated by a water molecule [36] and the Mg of BChl 5 is bound by the backbone oxygen of a leucine residue [37]. Only two of the seven assigned chlorophylls-a of LHC II, isolated from pea chloroplasts, are liganded by histidines. Of those remaining, four have their Mg atoms coordinated to acidic or amide residues and one is liganded to a backbone oxygen [18].

The B800 BChl-a of LH-2 of *Rs. molischianum* is found to be ligated to Oδ1 of α-Asp6; the distance between its central Mg and the Oδ1 of α-Asp6 is 2.45 Å. The other carboxyl oxygen of α-Asp6, Oδ, is in close proximity (2.75 Å) to the amide Nδ atom of α-Asn2, establishing a strong hydrogen bond between these residues. The binding site is presented in Figure 5b. A water molecule is located close (2.74 Å) to the Oδ1 of α-Asp6; this water also makes contact (at a distance of 3.10 Å) to the methyl-ester carbonyl oxygen O2 at ring V of the B800 BChl-a and a further contact (2.94 Å distance, not shown) to Nε2 of β-His17. A comparable water molecule has been found in LH-2 of *Rps. acidophila*, close to α-fMet1 and β-His12 [20]. In contrast to the B850 BChl-as, the binding environment for B800 BChl-a is polar. It is surprising that the B800 BChl-a has its optical absorption maximum at 800 nm in the LH-2 of both *Rps. acidophila* and *Rs. molischianum*, despite the fact that an aspartate is the Mg ligand in *Rs. molischianum* but a formyl-methionine in *Rps. acidophila*.

Figure 5

The bacteriochlorophyll binding pockets in the LH-2 of *Rs. molischianum*. **(a)** The B850 BChl-a pairs (cyan, with Mg in green) and surrounding aromatic residues. Tube representation of the α- and β-apoproteins (magenta and white, respectively) in the nearby region are also given as a reference frame. The numbers indicate distances in Å. **(b)** The binding pocket for B800 BChl-a and surrounding aromatic residues. Colours are as in (a). Dashed lines correspond to short distances to either the α (yellow) or the β (white) subunit, comprising possible hydrogen and metal bonds. **(c)** Pigments associated with two pairs of αβ-heterodimers in the LH-2 complex of *Rs. molischianum*: white, B850 BChl-as binding to α-subunits; cyan, B850 BChl-as binding to β-subunits; magenta, B800 BChl-as; yellow, lycopenes (LYC and LYC′). Surrounding aromatic residues are shown for one of the two lycopenes (LYC′). (Figure was produced with the program VMD [62].)
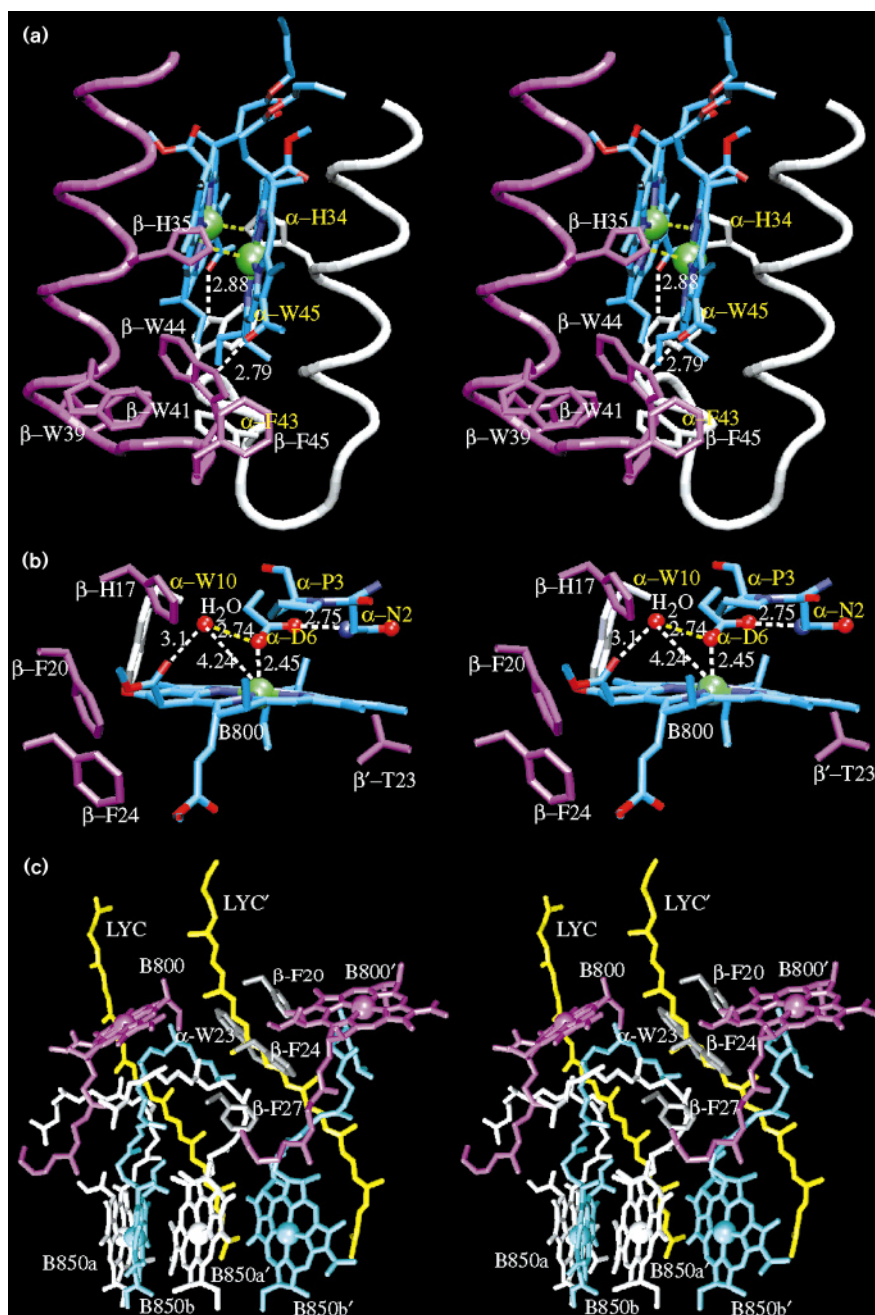
The α-Pro3 is most probably in *cis* conformation. The electron density close to the 2-acetyl carbonyl (O6) group of B800 BChl-a is modeled best by the side chain of α-Asn2. The carboxyl Oδ2 of the α-Asn2 forms weak hydrogen bonds to the amide side chain of β′-Gln19 of the neighbouring αβ-heterodimer. The amide Nδ atom of α-Asn2 is about 4 Å from the 2-acetyl carboxyl group of B800 BChl-a and, most importantly, the orientation is unfavorable for hydrogen-bond formation. At first glance, this appears to be in conflict with interpretations of Fourier

transform resonance Raman spectra [21]; these exhibit a shoulder at 1632 cm^{-1} suggesting a hydrogen bonded 2-acetyl carboxyl group. However, a hydrogen bond is likely between O6 of the B800 BChl-a and Oγ1 of β′-Thr23.

The suggestion of a hydrogen bonded 9-keto group for B800 BChl-a, gained from another shoulder in the Fourier-transformed Raman spectrum at 1678 cm^{-1}, is at variance with the electron density. No potential hydrogen-bond partner can be identified sufficiently close to the 9-keto

group oxygen (O1). In addition to β-His17, there exist three aromatic residues (β-Phe20, β-Phe24, α-Trp10) in the immediate surrounding of the B800 BChl-a, as shown in Figure 5b.

An interesting feature regarding the interactions of B800 BChl-a is its proximity to the phytyl tails of B850b and B850a′. A presentation in Figure 5c of two B800 BChl-as and four proximate B850 BChl-as shows how the well-resolved phytyl tails of B850b and B850a′ ascend towards B800 BChl-a, with a closest approach of 4 Å, and then descend again.

Carotenoid binding and function

The carotenoids absorb energy in a spectral region complementary to that of bacteriochlorophylls (BChls) and, most importantly, function as a photoprotective agent, quenching the BChl excited triplet state. This state would otherwise be long-lived and could readily react with molecular oxygen to generate singlet oxygen, which is extremely reactive and destructive [38,39]. Lycopene has been found to be the major carotenoid in the LH-2 complex of *Rs. molischianum* [21]; rhodopin has been identified as a minor component (<5%). The BChl-a to carotenoid ratio in LH-2 was estimated to be 2:1. However, only one lycopene per αβ-heterodimer can be identified in the crystal structure. This lycopene is in an all *trans* conformation, spanning the entire hydrophobic core of the transmembrane region. A long stretch (corresponding to a chain of about 10 carbons) of electron density near the B850a BChl-a has been tentatively assigned to a detergent molecule, but might correspond to a second lycopene, with partial occupancy.

Unlike many other carotenoids, lycopene does not have polar end groups. Interactions of conjugated polyene bonds of carotenoids with aromatic compounds suffice to hold the two components together [40]. As seen in Figure 5c, four aromatic residues (α-Trp23, β-Phe20, β-Phe24, β-Phe27) do indeed cluster in a localized zone around the lycopene within van der Waals contact of the lycopene (<5.0 Å), forming an anchor site for the chromophore.

Carotenoids quench triplet states of excited chlorophylls by the Dexter mechanism; the latter requires significant overlap of the wave functions of both molecules [5]. The crystal structure as presented in Figure 5c shows that lycopene is indeed in close contact (<5 Å) with the phytyl tails of the B850 BChl-as. Furthermore, the lycopene runs parallel (within 5 Å) to the porphyrin plane of B850a′, the B850 BChl-a bound to the α-apoprotein of the neighboring αβ-heterodimer. The lycopene from the neighboring αβ-heterodimer (labelled as LYC′ in Fig. 5c) makes van der Waals contact with the B800 BChl-a. Aromatic residues α-His34 and α′-Trp45 of the neighboring α-apoprotein are also in van der Waals contact with the lycopene.

Bound solvent molecules

When the concentration of detergents in water is low, but still above the critical micellar concentration, the detergents self-aggregate to micelles of spherical shape with the polar head-groups facing the surrounding bulk water and the hydrophobic hydrocarbon tails hidden in the inside [41]. The hydrophobic surface of the photosynthetic reaction center from *Rhodopseudomonas viridis* is coated by detergents that form ring-shaped micelles even in the crystalline state [42]. Hence, the polar head groups of the 'detergent belt' will cover a zone of the protein's polar surface adjacent to the hydrophobic surface of the membrane protein.

Small amphiphilic molecules like HPTO, used in our crystallization procedure, are believed to form mixed micelles with the detergent [11]. The effect of these molecules is similar to a shortening of the detergent's alkyl tail, that is, the small amphiphilic molecules are able to reduce the size of the micelle [25] and, thereby, might improve the quality of the crystal. At critical places on the surface of proteins they might replace detergent molecules. For crystallization, the detergent LDAO was replaced by the shorter UDAO in the presence of HPTO. These two molecules, as well as water molecules, are capable of binding to well-defined positions on LH-2. All three types of solvent molecules were identified in our structural analysis.

One UDAO molecule was fitted to an elongated stretch of electron density close to the B850 BChl-a. A piece of density in a similar orientation was found in the *Rps. acidophila* structure. This density was assigned to a detergent molecule [20], but remodelled as a fragment of a carotenoid in the coordinates made available to us. This UDAO molecule is located in a deep pocket on the outside of the octamer with its head group close to the C-terminal end of the membrane spanning helices. A well-defined HPTO molecule was found in another pocket on the outside surface of the octamer, between B800 and B850 BChl-a. Electron density that could be assigned to HPTO molecules appeared in the interfacial region of the octamers, filling small holes.

In one of the last refinement rounds, several pieces of electron density inside the core of the octamer were found. These densities have an elongated shape and are parallel to the z-axis. They can be assigned to three HPTO and one detergent molecule, as shown in Figure 6. The assigned HPTOs are in direct contact with the protein; the detergent molecule forms a second layer beyond the HPTO molecules. The existence of ordered solvent molecules in the core of the octamer may be an indication that lipid molecules fill the core of the LH-2 when it is embedded in the membrane. One could also raise the question of whether lipid molecules are still bound to the protein, but taking into account the strong detergent used in the

Figure 6

UDAO (detergent) molecules and small amphiphilic HPTO molecules, in their $2F_o–F_c$ electron density map at a contouring level of 0.7σ. HPTO molecules can be seen in the two layers in the upper part of the figure. Of the solvent molecules shown, one UDAO and three HPTO molecules belong to the crystallographic and NCS independent αβ-heterodimer. All other molecules were generated by crystallographic or NCS operators, to visualize the arrangement of extra electron density inside the hole of the octamer and its interpretation by solvent molecules.
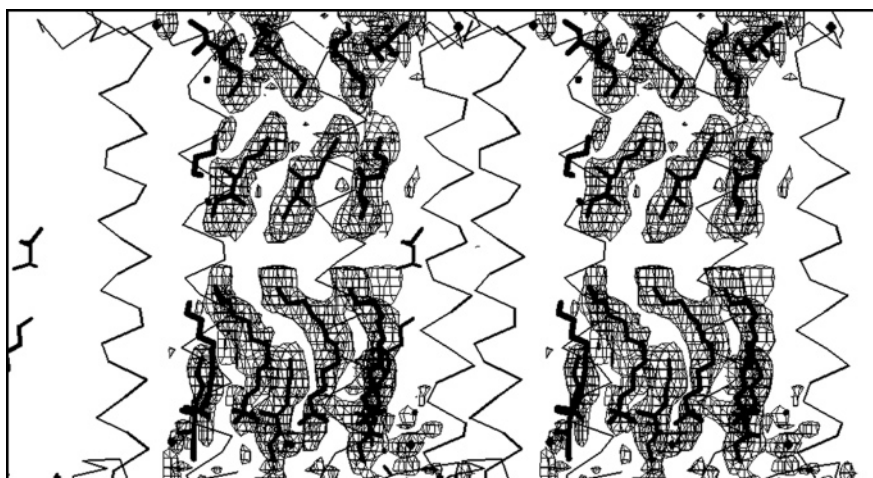
purification procedure and the various purification steps, it seems unlikely that this density is due to lipid molecules. It should be noted that the mentioned solvent molecules have a high temperature factor.

Water molecules were found only on the polar surface of the proteins or near the polar head groups of detergents and small amphiphilic molecules. Due to the limited resolution of our data, only water molecules in direct contact with the protein could be identified. Altogether, sixteen water molecules per αβ-heterodimer were refined.

Discussion

Comparison with _Rps. acidophila_ structure

LH-2 from _Rs. molischianum_ forms octamers instead of the nonamers observed in the _Rps. acidophila_ structure. In both structures, the modular αβ-heterodimers are circularly arranged, obeying strict rotational symmetry. The LH-2 from _Rs. molischianum_ appears to be more densely packed than that of _Rps. acidophila_. As a result, the B850 BChl-as are more tightly and evenly distributed in the circular ring; in _Rs. molischianum_, the Mg to Mg distance between neighboring B850 is 9.2 Å within the αβ-heterodimer and 8.9 Å between the heterodimers and the corresponding distances in _Rps. acidophila_ are 8.7 Å and 9.7 Å, respectively [20].

As demonstrated in Figure 7, which superposes the αβ-heterodimers of both LH-2s, both structures are very similar in the transmembrane region. Major differences are found at the N- and C-terminal ends. The α-apoprotein of _Rs. molischianum_ possesses a much longer C-terminal helix. This helix is at an angle of about 140° to the membrane spanning helix, compared with only about 100° in the _Rps. acidophila_ structure. The orientation of the N-terminal 3_{10} helices of the α-apoproteins are remarkably similar, despite this helix being longer in _Rs. molischianum_

and having different contacts to B800 BChl-a. The N terminus of the β-apoprotein is ill defined and therefore differences in this part are less significant.

As seen in Figure 7, essential differences are observed in the orientation of BChl-a phytyl chains. The B800 BChl-a porphyrin rings of the two LH-2s are tilted with respect to each other by about 20°. Furthermore, the two B800 BChl-as are found to be rotated by 90° relative to each other in the plane of the porphyrin ring. Accordingly, the Q_y transition dipole moment of B800 BChl-a of _Rs. molischianum_ is parallel to the respective transition dipole moment of the B850 BChl-a attached to the same apoproteins, whereas the corresponding transition dipole moments are nearly perpendicular in _Rps. acidophila_. Our attempt to place the B800 BChl-a of the _Rs. molischianum_ LH-2 in the same orientation as in the crystal structure of LH-2 of _Rps. acidophila_ induced a significant bend of the tetrapyrrole ring in B800 BChl-a and led to a rise in the free R-value, and was abandoned.

Although the carotenoid molecules are different (lycopene in _Rs. molischianum_ versus rhodopin-glucoside in _Rps. acidophila_), they adopt a similar orientation in both structures with only minor deviations close to the B850 BChl-as.

Internal energy transfer

The LH-2 complex converts all light absorbed into Q_y excitations of B850 BChl-a. The transfer of light energy between the B800 BChl-as and B850 BChl-as occurs on a subpicosecond time scale [6,43]. This short time scale may arise from concerted action of the Dexter and Förster mechanisms [44]. The Dexter mechanism could occur through exchange interactions mediated by lycopenes and possibly by the B850b phytyl tail (see Fig. 5c and above). The Förster mechanism [44,6] is most effective when the Q_y transition dipole moments of B800 BChl-a and its most

Figure 7
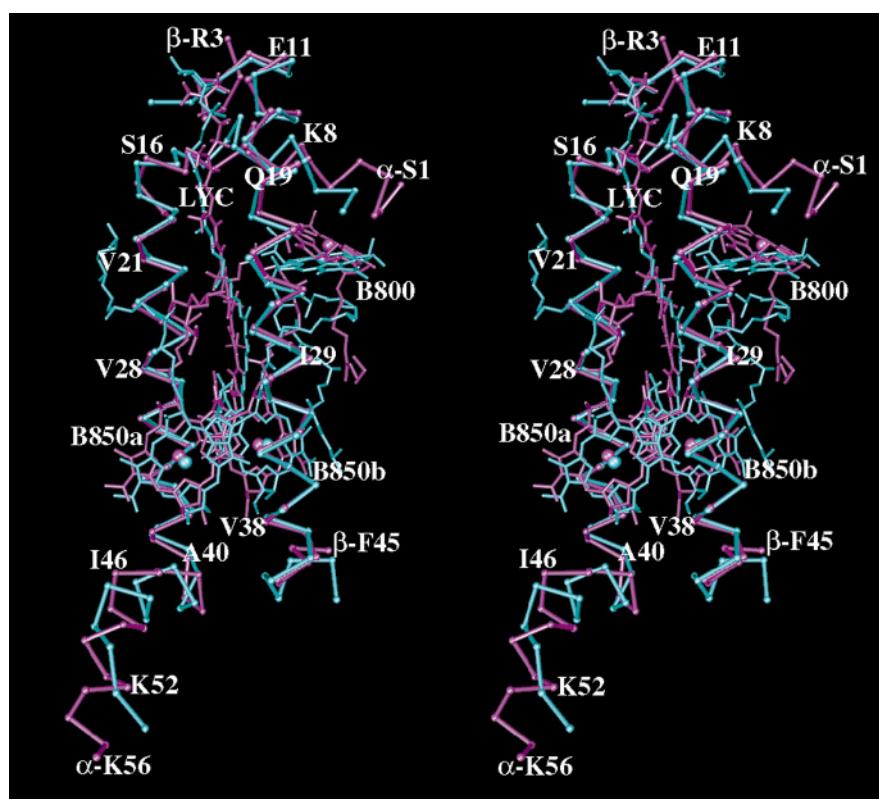
Superposition of the structures of LH-2 from *Rs. molischianum* (magenta) and from *Rps. acidophila* (cyan). The apoproteins are displayed as Cα traces. The B800 and B850 BChl-as, lycopene (LYC) and residues for LH-2 of *Rs. molischianum* are labeled. (α and β prefixes were used for some residues to avoid ambiguities.)

proximate B850b or B850a′ (see Fig. 5c) are colinear or at least parallel; the Mg–Mg distances to B850b and B850a′ (20.2 Å and 19.1 Å, respectively) can be readily bridged. The structure of LH-2 of *Rs. molischianum* reveals that these transition dipole moments are parallel. To arrive at this conclusion we note that the Q_y transition dipole lies along the molecular Y-axis of chlorophyll, that is, the axis connecting the N atom of pyrrole I and the N atom of pyrrole III [45,46]. The Q_y transition dipole moment of B800 BChl-a in LH-2 of *Rs. molischianum* then forms angles of 13.1° and 151.5° with the respective transition dipole moments of B850b and B850a′. Figure 8 presents the Q_y and Q_x transition dipole moments of LH-2 of *Rs. molischianum* in a projection onto the membrane plane.

Although the planes of the B800 BChl-a rings are not parallel to the plane of the membrane, the Q_y transition dipole moments of these BChl-as are parallel to the membrane plane to within 10°, which is in agreement with recent observations [47].

How far is the ring-like architecture of LH-2 optimal for the protein's function? The cyclic assembly of 24 chlorophylls and eight, possibly more, lycopenes divides into three functional units: the lycopenes, the B800 BChl-as and the B850 BChl-as. The relevant excited states of lycopenes

and B800 BChl-as are energetically distant from each other and only weakly coupled through interactions between induced dipoles. One may therefore consider these chromophores as sixteen independent units that absorb light in their respective spectral ranges and transfer the light energy to the B850 BChl-a system. The lycopenes are in closer contact with the chlorophylls, but as their excited states lie at significantly higher energy, they can still be considered to act like individual chromophores.

The unit of 16 B850 BChl-as functions through coherent superpositions, so-called excitons, of the relevant Q_y excited states of individual chlorophylls, the cyclic arrangement being optimal for energy transfer. The excitons arise through the interactions of adjacent B850 BChl-as, which, when considered pairwise, resemble the special pair in the photosynthetic reaction center (RC) of *Rps. viridis* [13]. The interaction energy (V_p) for the special pair can be estimated from observed spectra and is 500 cm^{-1} [48]; the respective interactions in LH-2 should be weaker, say $V_p \approx 400$ cm^{-1}, due to the larger Mg–Mg distances (~7 Å in RC and ~9 Å in LH-2 of *Rs. molischianum*).

The excitons can be estimated from an approximate quantum mechanical description of the sixteen B850

Figure 8
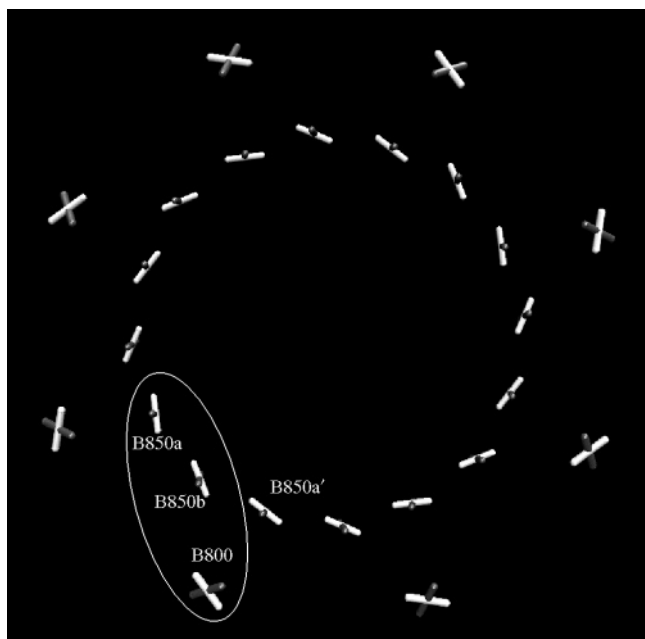
Orientation of Q_y and Q_x transition moments of bacteriochlorophylls. The Q_y transition moment (white) is defined by the vector connecting the N atom of pyrrole I and the N atom of pyrrole III. The Q_x transition moment (silver) is defined by the vector connecting the N atom of pyrrole II and the N atom of pyrrole IV. Encircled BChl-as represent one basic unit.

chlorophylls through an elementary calculation which resembles the description of vibrations of a circular string of sixteen beads. For this purpose one needs to establish the so-called Hamiltonian, a 16×16 matrix in the present case, the dominant elements of which are the diagonal and the first off-diagonal elements; other matrix elements accounting for non-nearest neighbour interactions can be assumed to vanish; a more complete description requires an extended quantum chemical calculation. The so-called eigenvalues and eigenvectors of the Hamiltonian matrix yield the excitation energies and excitons of the B850 system from which, in particular, the dipole strength governing absorption into and emission out of the exciton system can be determined. Labeling the sixteen B850 BChl-as by j, one can compose the excitons from the states $|\tilde{j}\rangle$, in which all chromophores are in the ground state except for the chromophore j which is in the Q_y excited state. The exciton states manifest themselves as the coherent superpositions $|N\rangle = \Sigma_j \gamma_{Nj} |\tilde{j}\rangle$ (N=0, 1, ...15) and can be determined as the eigenstates of the 16×16 Hamiltonian matrix $H_{jj} = \langle \tilde{j} | H | \tilde{j}' \rangle$ which describes how any state $|\tilde{j}\rangle$ is coupled to any state $|\tilde{j}'\rangle$, the diagonal elements H_{jj} being given by the excitation energies E_y of the individual chlorophyll Q_y states. As the Mg atoms of sixteen B850 BChl-as are located approximately on the vertices of a hexadecamer, the coefficients

γ_{Nj} can be approximated by $\gamma_{Nj} = \frac{1}{4} \exp(i\pi jN/8)$. The notation used here is that of standard textbooks, for example, that of [49]; excitons of circular assemblies of chlorophylls have been described in [50,51] and for the present system in [52].

For the arrangement of the chlorophylls in LH-2, the Hamiltonian $H_{jj'}$ is dominated by the interactions $H_{jj\pm1} = V_p$ between excitations of neighbouring chlorophylls. Neglecting other interactions, the exciton states increase in energy in the order $E_y - 2V_p$ (one state), $E_y - 2V_p\cos(\pi/8)$ (two states), $E_y - 2V_p\cos(2\pi/8)$ (two states), ... $E_y + 2V_p$ (one state). A more detailed analysis reveals that for the idealized geometry only the two states with energy $E_y - 2V_p\cos(\pi/8)$ absorb light with perpendicular transition dipole moments, that is, they absorb light from all directions with equal strength. These states then absorb at about 50 nm, that is, $2V_p\cos(\pi/8)$. This is to the red of the absorption of the individual chlorophylls (850 nm), if the latter are assumed to absorb at E_y=800 nm. These two states lie only $2V_p[1-\cos(\pi/8)] \approx 0.15$ kcal mol^{-1} above the energetically lowest exciton state at $E_y - 2V_p$, which is optically forbidden and hence conserves light energy. After absorption of light by LH-2, energy is channeled to the exciton states which equilibrate very rapidly; the optically allowed excitons remain well populated as their Boltzmann factor, exp(-0.15 kcal mol kT^{-1}) ≈ 0.8, is sufficiently high. Hence, the exciton band transfers light energy efficiently to LH-1 and to the photosynthetic reaction center. This optimal scenario can be reversed, in case the arrangement of B850 chlorophylls is altered such that the optically allowed exciton states become thermally inaccessible. In this case, the protein would dissipate absorbed light energy. The ring architecture of chlorophylls is likely to stimulate more focused theoretical and spectroscopic studies in the years to come.

Conserved residues

Multiple sequence alignments of LHs [21,22] reveal three highly conserved histidine residues. Two of the three histidines are the ligands binding to the Mg atoms of B850 BChl-as, and the third histidine forms part of the B800-binding pocket. These structural features are consistent with site-directed mutagenesis experiments of LH-2 from *Rb. capsulatus* and *Rb. sphaeroides* [53–55]. The motif α-Ala30...α-His34...α-Leu38 is highly conserved. The corresponding alanine (at position −4 relative to the conserved histidine) in LH-1 of *Rb. capsulatus* can only be substituted with the small residues glycine, serine and cysteine [53]. A similar binding pocket β-Phe27...β-Ala31...β-His35 is also highly conserved in the β-apoprotein. The conserved phenylalanine residue in the −8 position to His35 forms part of the binding site for lycopene and B850 BChl-a. The two conserved tryptophan residues, α-Trp45 and β-Trp44, are hydrogen bonded to the 2-acetyl groups of the B850 BChl-as.

Tryptophan residues are abundant in the lipid–water interfaces. Four tryptophan residues per αβ-heterodimer are clustered near the periplasmic interface and three are found at the cytoplasmic interface. Similar observations have been made for the photosynthetic RCs [14,56], demonstrating the importance of these residues for the structure of membrane proteins.

Biological implications

Light harvesting complexes (LHs) are part of the photosynthetic apparatus of plants and photosynthetic bacteria. The complexes function as light gathering antennae and transfer the light energy to the photosynthetic reaction center. When exposed to direct sunlight, chlorophylls absorb at a rate of at most 10 Hz and in dim light, at a rate of 0.1 Hz. On the other hand, the reaction center can cycle at 1000 Hz [57]. Energy transfer from antenna complexes to the reaction center can therefore increase the efficiency of energy utilization by two orders of magnitude, and broaden the spectral range of light used. This requires that the architecture of the LHs is flexible, allowing the complexes to aggregate around the photosynthetic reaction center. The result is a cascade of absorption energies that funnels the light energy. The efficiency of the LHs must be adapted to high light intensities to avoid burning of the photosynthetic reaction centers.

The structure of LHs provides the information necessary for understanding energy transfer in the photosynthetic membrane. Structural information is particularly important as the architecture of the LHs is unusual, the proteins being ring-like oligomers formed by individual α-helical segments with which two bacteriochlorophyll-a molecules (BChl-as) absorbing at 846 nm (B850), one Bchl-a absorbing at 800 nm (B800) and the major carotenoid, a lycopene (LYC), are associated.

Light harvesting involves absorption of light over a broad spectral range, internal conversion into electronic excitation of the Qy exciton transition states of bacteriochlorophyll-a molecules and further energy transfer. The understanding of physical mechanisms underlying these processes requires a detailed knowledge of chromophore orientation and contacts. For example, for *Rhodospirillum molischianum* we have shown that that the Q_y transition dipole moment of the B800 BChl-a is nearly parallel to that of the neighboring B850 BChl-a; this alignment is optimal for energy transfer through Förster mechanism. Furthermore, the structural arrangement of the carotenoids in LH-2 of *Rs. molischianum* illustrates well how carotenoids function as both light harvesting pigments and photoprotection agents. Another example is the finding that the binding environment of the B850 BChl-a is non-polar, whereas of B800 BChl-a is polar. This information will be helpful in understanding how *in vivo* **chromophore–protein interactions produce the spectral shifts vital to the cascade of excitation energies by which light is funneled in the photosynthetic system.**

Material and Methods

Crystallization

The growth of *Rs. molischianum* and the purification of its LH-2 have been described elsewhere [21]. The material eluted from the final Mono-Q FPLC column (Pharmacia) was dialysed overnight against 100 volumes of 10 mM phosphate buffer, pH 8.7, containing 0.1% (w/v) LDAO (Fluka) as detergent and 0.1% (w/v) sodium azide. In order to exchange the detergent, the LH-2 was absorbed onto a small (3 ml) ion exchange column (Q-Sepharose fast flow, Pharmacia) pre-equilibrated with the buffer mentioned above and washed with 25 ml of the same buffer but containing 0.2% (w/v) UDAO (Oxyl, Bobingen, Germany) instead of LDAO. The LH-2 was eluted with 150 mM potassium phosphate buffer at pH 6.5 containing 0.2% (w/v) UDAO and 0.1% sodium azide. It was then concentrated to an absorbance of 200 at 850 nm, corresponding to 20 mg ml^{-1}, using Amicon filtration cells or Centricon tubes (Amicon). 3.2% (w/v) HPTO (high melting isomer, Oxyl or Fluka) and the same volume of 4 M ammonium sulfate were added. 50 μl droplets were equilibrated against 8 ml 3.0–3.3 M ammonium sulfate using the sitting drop technique at 20°C. Single crystals, up to 3 mm in length, appeared within about four to eight weeks, but were rare. Under these conditions HPTO is also under supersaturation.

Data collection

X-ray intensity data were collected from a single crystal using synchrotron radiation with 1.009 Å wavelength at the HASYLAB station X31. As the space group was P42$_1$2, the crystals were rotated around their c-axis by 45° for collecting a high resolution (step size 1.2°) and a low resolution (step size 4.5°) dataset. Two datasets needed to be collected due to the limited dynamic range of the MarResearch image plate area detector prototype. With a completeness of over 80 % for significant observations [F>2σ(F)], the crystal diffracted to 2.4 Å resolution. Data were processed with the DENZO data reduction program of the HKL program suite [58,59]. The processed data were merged using the SCALEPACK program. Structure factors were calculated from the measured intensities employing the program TRUNCATE from the CCP4 package [60] and an overall temperature factor B$_{Wilson}$ was determined. The relevant crystallographic data are summarized in Table 1.

Molecular replacement

The α- and β-subunits of LH-2 of *Rs. molischianum* are homologous to those of LH-2 of *Rps. acidophila* (26% and 31% overall identity for the α- and the β-subunit, respectively; 46% and 35% identity for the respective transmembrane regions α-Lys8 to α-Ala39 and β-Leu8 to β-Trp44 of *Rs. molischianum*). The sequence alignments for the two apoproteins are provided in Figure 9. Despite the close homology of the transmembrane segments, direct use of a simple homology model to LH-2 of *Rps. acidophila* in the molecular replacement method was not possible as LH-2 of *Rs. molischianum* is an octamer, whereas LH-2 of *Rps. acidophila* is a nonamer. One important characteristic of this octamer is its eightfold symmetry, as revealed by a self-rotational analysis of the diffraction data. As shown in the contour plot of the self-rotational function presented in Figure 10, a peak at φ=90°, ψ=90° and κ=45° in the spherical polar coordinate system, as implemented in X-PLOR [30], clearly exhibits an eightfold symmetry axis parallel to the z-axis. We have adapted the molecular replacement method to the present case, employing model building to generate, in a two step procedure, an octameric structure as a search model.

In a first step, structures of the α- and β-apoproteins were determined by means of homology modeling using the apoproteins of *Rps. acidophila* LH-2 as a template. As close homology between LH-2 of *Rs. molischianum* and of *Rps. acidophila* exists only for the transmembrane segments of the apoproteins, we sought further templates for the extramembrane region, using sequence homology and secondary

Figure 9

(a) Sequence alignment of the α- and β-apoproteins by BLAST [74]. (b) Alignment of homologous segments for homology modeling: 1R1E, Eco RI endonuclease (E.C.3.1.21.4) complexed with TCGCGAATTCGCG; 1TYP, trypanothione reductase (E.C.1.6.4.8); 1AAM, aspartate aminotransferase (E.C.2.6.1.1) mutant; 2RCR, photosynthetic reaction center from *Rhodobacter sphaeroides*. The ratios give the first and the last number of the residues used for the alignment, in the frame of the respective sequence.

```
(a)                                      α-apoprotein
Rs. molischianum   SNPKDDYKIWLVINPSTWLPVIWIVATVVAIAVHAAVLAAPGFNWIALGAAKSAAK
Alignment                  KIW V+NP+   +P +    TV+AI VH A+L+
Rps. acidophila    ---MNQGKIWTVVNPAIGIPALLGSVTVIAILVHLAILSHTTWFPAYWQGGVKKAA

                                         β-apoprotein
Rs. molischianum   AERSLSGLTEEEAIAVHDQFKTTFSAFIILAAVAHVLVWVWKPWF-
Alignment                 LT E++  +H        F+ LA VAH L +    PW
Rps. acidophila    -----ATLTAEQSEELHKYVIDGTRVFLGLALVAHFLAFSATPWLH

(b)                                      α-apoprotein
Rs. molischianum   1:56     SNPKDDYKIWLVINPSTWLPVIWIVATVVAIAVHAAVLAAPGFNWIALGAAKSAAK
1R1E               97:106   ---KDDYGEWRVV--------------------------------------------
Rps. acidophila    5:36     -------KIWTVVNPAIGIPALLGSVTVIAILVHLAILS-----------------
1TYP               91:102   -------------------------------------------NWKALIAAKNKA-

                                         β-apoprotein
Rs. molischianum   1:45     AERSLSGLTEEEAIAVHDQFKTTFSAFIILAAVAHVLVWVWKPWF
1AAM               349:365  ---SFSGLTKEQVLRLREEF-------------------------
Rps. acidophila    3:39     ------LTAEQSEELHKYVIDGTRVFLGLALVAHFLAFSATPW-
2RCR               266:272  -----------------------------------WVKLPWW
```

structure identity as search criteria. In this respect, a consensus assignment for the secondary structure of the α- and β-apoprotein of *Rs. molischianum (*from an earlier investigation of homology building of the same structure) proved to be useful [22]. The homologous fragments employed are shown in Figure 9. Homology modelling was performed using the program MODELLER [61] and the molecular graphics package VMD [62,63].

In a second step, the αβ-heterodimers obtained were aggregated into an octameric complex by means of energy minimization and molecular dynamics simulations under the constraint of an eightfold symmetry axis. The implementation has been reported in [22]. Starting from different initial octameric configurations, five model structures were built.

The modeled structures served as search models in the framework of the molecular replacement method as implemented in X-PLOR [30]. The method is actually implemented as a 3D rotational search followed by a 3D translational search as a full six-dimensional search is too time consuming [64,65]. Before the translational search, we performed a Patterson correlation (PC) refinement to filter the peaks of the rotational search [66].

Table 1

Summary of the crystallographic data.

Space group	P42$_1$2
Unit cell	
a=b (Å)	91.60
c (Å)	209.97
N*	4
Solvent content (%)	70.7
B$_{Wilson}$ (Å^2)†	47
Resolution range (Å)	8.0–2.4
Unique reflections	30 309
Completeness (%)	87.2
R-symm (%)	9.7
R-factor (%), F>2σ(F)	21.1
Free R-factor (%)‡	23.2
Solvent	
Detergent molecules	3
HPTO molecules	6
Water molecules	16

*N gives the number of αβ-heterodimers per asymmetric unit. †B$_{Wilson}$ is an estimate of the average temperature factor for the crystal. ‡The free R-value is calculated from the 7% of the measured unique data that were not used during refinement.

One of the five search models successfully oriented and positioned one octamer in the unit cell with unique rotational and translational peaks. With the eightfold axis of the search model initially oriented parallel to the z-axis of the unit cell, the N termini pointing upward, the rotational search identified an orientation with Euler angles $(\theta,\phi,\psi)=(6°,0°,0°)$, which was refined by PC correlational search to (4.9°,0°,0°). An Euler angle $\phi=0°$ signifies here that the octamer prefers an orientation in which the eightfold axis of the octamer remains parallel to the z-axis. The subsequent translational search resulted in fractional coordinates $(x,y,z)=(0.0,0.5,0.38)$ of the center of the octamer with its eightfold axis aligned with the fourfold symmetry axis of the space group P42$_1$2.

The resulting position in the unit cell is shown in Figure 11 at position 1. Due to the crystal symmetry one must complement this LH-2 by the one shown at position 1′, that is, the search actually determined two LH-2s related by crystallographic symmetry. However, it has been determined that there are four LHs in the unit cell, based on density arguments [21]. Indeed, the unit cell can be divided into four layers (see Fig. 11), each 52.5 Å thick, and therefore would readily accommodate four transmembrane proteins. Hence, one expects that two further LH-2s exist in the unit cell (e.g. those indicated at positions 2 and 2′ in Fig. 11). Their existence raises the question of why positions 2 and 2′ did not reveal themselves in the molecular replacement search described above.

In principle, the missing mates could be detected through a so-called self-rotational search. Figure 11, which presents the crystal packing as emerged ultimately in this study, indicates why this search failed. If, as shown, the mates 2 and 2′ are positioned in close contact to the LH-2s at positions 1 and 1′, respectively, then inter- and intramolecular distances cannot be distinguished well for the pairs 1, 2 and 1′, 2′. Accordingly, as demonstrated in Figure 10b, self rotational search was unable to produce any twofold NCS rotational axis in the asymmetric unit that is not overlapping with the crystal symmetry axes. Self-rotational search relies on self-Patterson vectors being intramolecular and, thus, shorter than cross-Patterson vectors which have intermolecular origin. In principle, it is possible for the twofold NCS axis to overlap with the crystal twofold or fourfold axes. That possibility was ruled out later.

An ultimate alternative is a combined translational and rotational search of two independent LH-2s, that is, a 12-dimensional search. To overcome the resulting computational barrier, we restricted the search to two independent translations along the z-axis, Z_1, Z_2, and to two independent rotations around the z axis, θ_1,θ_2. By doing this, the orientation of the two octamers was assumed to be parallel or antiparallel to the z axis of the unit cell and the central symmetry axis of the octamers was assumed to be overlapping with the crystal fourfold axis, such that the
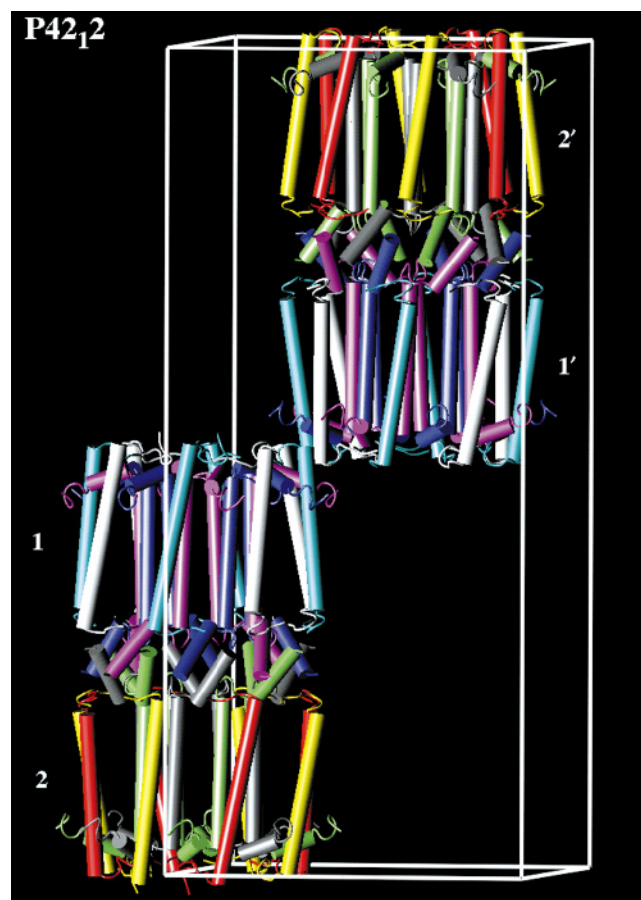
Figure 10
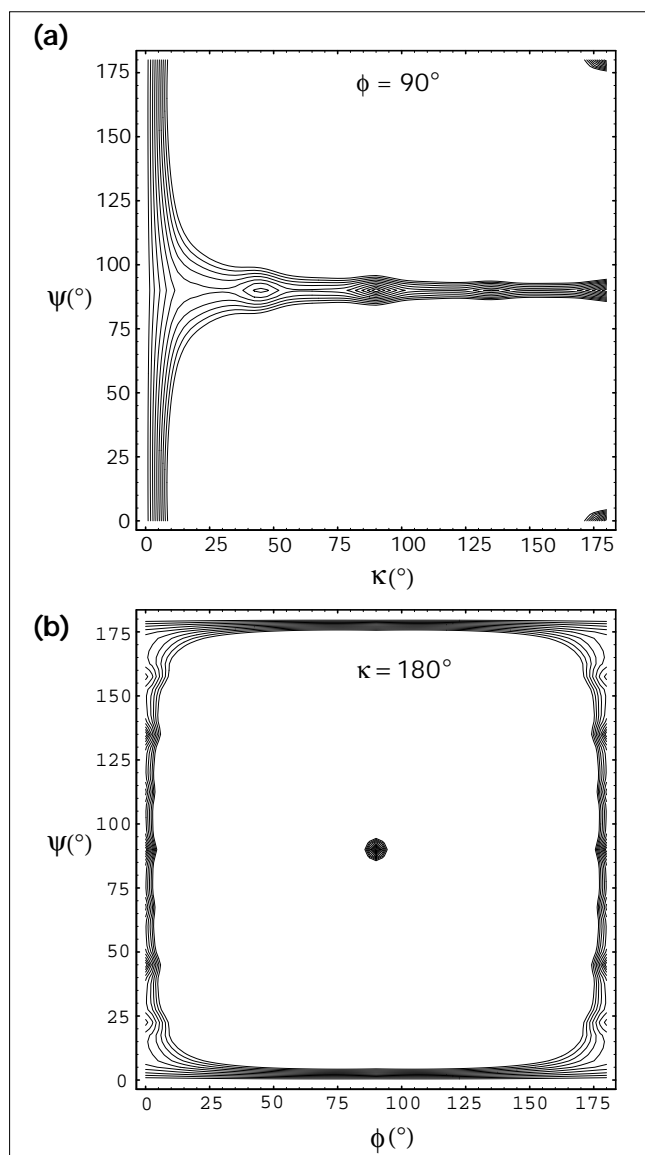
Contour plot showing the self-rotational function of LH-2 diffraction data at 12–4 Å resolution, using the spherical polar coordinate system as implemented in X-PLOR. ϕ is held fixed at 90° for the top panel; κ is held fixed at 180° for the bottom panel.

octamers assume fixed fractional coordinates (x,y) of (0,0.5) or (0.5,0). The first octamer was placed initially in an orientation and position as found by the conventional molecular replacement method, that is, the octamer was centered at (0.0,0.5,0.38), which defines $Z_1=0$ Å and $\theta_1=0°$. The second octamer was oriented initially parallel to the first one, but centered at (0.5,0.0,0.88), which defines $Z_2=0$ Å and $\theta_2=0°$. The E_2E_2 (see [30]) correlation coefficient with 4–12 Å resolution data was chosen as the target function for the direct search as it correlates well with the accuracy of phases [67].

The search proceeded as follows. A coarse grain search was conducted varying θ_1, θ_2 between 0° and 45° in steps of 2.5° and Z_1 and Z_2 between −78.75 Å and +26.25 Å in steps of 5 Å. This confined the positions to the vicinity of $Z_1=0$ Å, $\theta_1=45°$, $Z_2=0$ Å, $\theta_2=27.5°$. A finer

Figure 11

Crystal packing in the unit cell. The cylinders represent helical segments of apoproteins in LH-2 complexes. LH-2s related by crystallographic symmetry, that is, 1 and 1′, 2 and 2′, are represented in identical colors. (Figure was produced with the program VMD [62].)

search near these positions in steps of 1° and 1 Å led to a successful solution. Figure 12 presents the maxima in the E_2E_2 correlation coefficient to demonstrate the quality of the results. The correlation coefficient exhibits a very sharp peak of 0.35 at $Z_1=−3.0$ Å, $\theta_1= 45°$, $Z_2= −4.0$ Å, $\theta_2=28°$.

The asymmetrical unit [½a×½b×½c] combines a motif from an octamer centered at (0.0,0.5,0.365) and the crystallographic symmetry mate of the motif from the other octamer centered at (0.5,0.0,0.861).

NCS averaging
To improve the quality of the phases, real space density averaging was carried out with the RAVE software package [68]. The four NCS operators were defined initially by a first model which was generated after one round of rigid body minimization to the solution of direct search. Later, they were improved by the IMP program in the RAVE package. A mask was generated from the PDB file of the protomer, using the mask-manipulation program MAMA. Typically, in the final stage of refinement, ten cycles of averaging of the $2F_o$–F_c map with RAVE resulted in an improved map with an overall R-factor of 16.6% and correlation coefficients of 0.94 to 0.95 between the protomer and three NCS symmetry-mates. We used the NCS averaged density map mainly to guide the manual adjustment of terminal residues and of the phytyl tails of BChl-a.

Figure 12

Results of the combined rotational and translational search. **(a)** E_2E_2 correlation coefficient as a function of Z_2 and θ_2 with $Z_1 = -3.0$ Å and $\theta_1 = 45°$. **(b)** E_2E_2 correlation coefficient as a function of θ_1 and θ_2 with $Z_1 = -3.0$ Å and $Z_2 = -4.0$ Å.
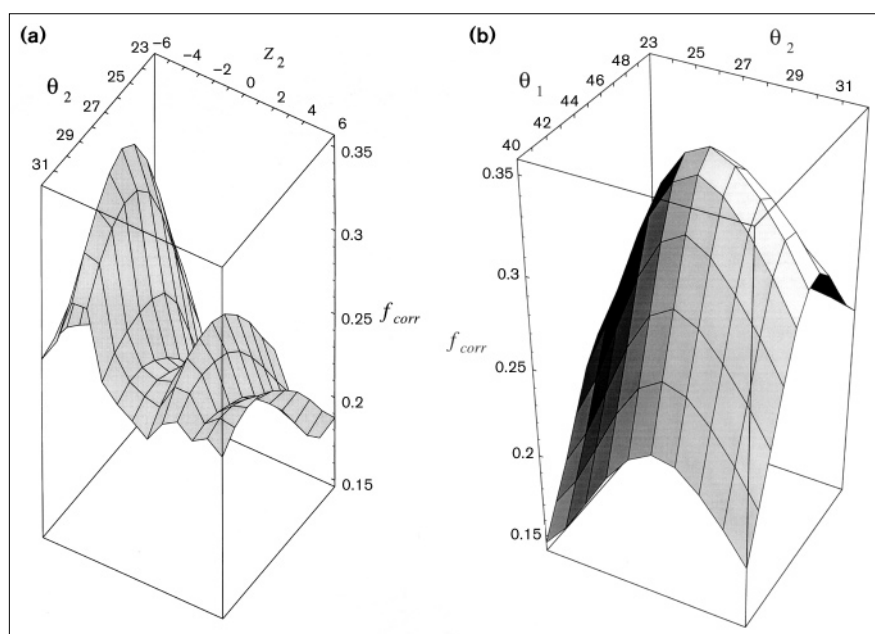
Refinement

Refinement was carried out with X-PLOR [30], using the Engh and Huber parameter set [69]. Parameter and topology files for BChl-a, generated according to the procedure outlined by Engh and Huber, were used earlier [70]. Parameter sets for the carotenoid (lycopene), the detergent molecule, and HPTO were constructed within the program QUANTA and INSIGHT-II using the respective CHARMm [71] force fields.

An initial model was constructed from the solution of a direct search, as described above. The asymmetrical unit contains two motifs from two crystallographically independent LH-2 octamers. Each motif consists of two αβ-heterodimers which are related by a non-crystallographic eightfold rotational axis. Refinement was carried out initially for data from 12 Å to 3 Å resolution. A rigid-body refinement of the initial model converged to a conventional R-value of 39%. The resulting co-ordinates for the four, symmetry independent, αβ-heterodimers then served as a basis for the calculation of NCS matrices. Strict NCS was enforced thereafter, and NCS matrices were eventually improved using the RAVE real space averaging package [68,72].

7% of the measured data were marked for a test set to calculate the free R-value [31,32]. Simulated annealing was performed using the standard slow cooling protocol (temperature bath coupling, molecular dynamics from T=4000 K to 300 K with velocity scaling every 25 fs, and integration time step of 0.5 fs) [30]. In the later stage of refinement temperature factors were refined after each annealing run. The free R-value was monitored throughout the procedure and was found to always improve in parallel with the conventional R-value.

Refinement was interlaced with model building sessions using the program O [28]. NCS averaged maps generated with the RAVE package served as a guide if the 2F$_o$–F$_c$ maps were unclear. After addition of a carotenoid molecule and missing residues at the N and C termini of the apoproteins, 1021 non-hydrogen atoms were refined against 17172 structure factors. Refinement was then carried out at the full resolution of 2.4 Å against 30309 unique reflections as temperature factors for each non-hydrogen atom were released. Only at 2.4 Å resolution could the orientation of the B800 chlorophyll be identified. The addition of some detergent and HPTO molecules brought further improvement. In the later stages of refinement water molecules were added. For the identification of solvent molecules, F$_o$–F$_c$ difference maps were searched for the highest peaks using the program O [28].

Originally, from chemical sequencing, it was suggested that residue 43 of the α-apoprotein was a serine [21]. However, the electron density was not compatible with a serine, but with a larger aromatic residue. Subsequent sequencing of the DNA [73] revealed a codon for phenylalanine in the corresponding position, which is in full agreement with the electron density. In the final round of refinement, the first two residues of the β-apoprotein and the last 11 carbon atoms of the phytyl-chain of B800 BChl-a were deleted, as their temperature factors refined in previous rounds to extremely high values. Finally, refinement converged to a free R-value of 23.2% and a conventional R-value of 21.1% (see Table 1).

Accession numbers

The coordinates of the structure have been deposited in the Brookhaven Protein Data Bank and issued the ID code 1LGH, for release one year from the date of publication.

References

1. Zuber, H. (1985). Structure and function of light-harvesting complexes and their polypeptides. *Photochem. Photobiol.* **42**, 821–825.
2. Zuber, H. (1993). Structural features of photosynthetic light-harvesting systems. In *The Photosynthetic Reaction Center*. (Deisenhofer, J. & Norris, J.R., eds), pp. 43–100, Academic Press, San Diego.
3. Karrasch, S., Bullough, P. & Ghosh, R. (1995). 8.5 Å projection map of the light-harvesting complex I from *Rhodospirillum rubrum* reveals a ring composed of 16 subunits. *EMBO J.* **14**, 631–638.
4. Kramer, H.J.M., van Grondelle, R., Hunter, C.N., Westerhuis, W.H.J. & Amesz, J. (1984). Pigment organization of the B800-850 antenna complex of *Rhodopseudomonas sphaeroides*. *Biochim. Biophys. Acta* **765**, 156–165.

5. Dexter, D. (1953). A theory of sensitized luminescence in solids. *J. Chem. Phys.* **21**, 836–850.
6. van Grondelle, R., Dekker, J., Gillbro, T. & Sundstrom, V. (1994). Energy transfer and trapping in photosynthesis. *Biochim. Biophys. Acta* **1187**, 1–65.
7. Cogdell, R.J., Durant, I., Valentine, J., Lindsay, J.G. & Schmidt, K. (1983). The isolation and partial characterization of the light-harvesting pigment–protein complement of *Rhodopseudomonas acidophila. Biochim. Biophys. Acta* **722**, 427–455.
8. Welte, W., *et al.*, & Drews, G. (1985). Crystallization of the photosynthetic light-harvesting pigment–protein complex B800–850 of *Rhodopseudomonas capsulata. FEBS Lett.* **182**, 260–264.
9. Wacker, T., *et al.*, & Welte, W. (1986). Crystallization and spectroscopic investigation with polarized light of the reaction center–B875 light-harvesting complex of *Rhodopseudomonas palustris. FEBS Lett.* **197**, 267–273.
10. Papiz, M.Z., *et al.*, & Lindsay, J.G. (1989). Crystallization of two crystal forms of the B800–850 light-harvesting complex from *Rhodopseudomonas acidophila* strain 10050. *J. Mol. Biol.* **209**, 833–835.
11. Michel, H. (1991). General and practical aspects of membrane protein crystallization. In *Crystallization of Membrane Proteins*. (Michel, H., ed), pp. 74–88, CRC Press, Boca Raton, FL.
12. Ghosh, R., *et al.*, & Rosenbusch, J.P. (1993). Two-dimensional crystallization of the light-harvesting complex from *Rhodospirillum rubrum. J. Mol. Biol.* **231**, 501–504.
13. Deisenhofer, J., Epp, O., Miki, K., Huber, R. & Michel, H. (1985). Structure of the protein subunits in the photosynthetic reaction center of *Rhodopseudomonas viridis* at 3 Å resolution. *Nature* **318**, 618–624.
14. Deisenhofer, J. & Michel, H. (1989). The photosynthetic reaction centre from the purple bacterium *Rhodopseudomonas viridis. EMBO J.* **8**, 2149–2170.
15. Komiya, H., Yeates, T.O., Rees, D.C., Allen, J.P. & Feher, G. (1988). Structure of the reaction center from *Rhodobacter sphaeroides* R-26 and 2.4.1: symmetry relations and sequence comparison between different species. *Proc. Natl. Acad. Sci. USA* **85**, 9012–9016.
16. Chang, C.-H., El-Kabbani, O., Tiede, D., Norris, J. & Schiffer, M. (1991). Structure of the membrane-bound protein photosynthetic reaction center from *Rhodobacter sphaeroides. Biochemistry* **30**, 5352–5360.
17. Ermler, U., Fritzsch, G., Buchanan, S. K. & Michel, H. (1994). Structure of the photosynthetic reaction centre from *Rhodobacter sphaeroides* at 2.65 Å resolution: cofactors and protein-cofactor interactions. *Structure* **2**, 925–936.
18. Kühlbrandt, W., Wang, D.-N. & Fujiyoshi, Y. (1994). Atomic model of plant light-harvesting complex by electron crystallography. *Nature* **367**, 614–621.
19. Montoya, G., Cyrklaff, M. & Sinning, I. (1995). Two-dimensional crystallization and preliminary structure analysis of light harvesting II (B800–850) complex from the purple bacterium *Rhodovulum sulfidophilum. J. Mol. Biol.* **250**, 1–10.
20. McDermott, G., *et al.*, & Isaacs, N. (1995). Crystal structure of an integral membrane light-harvesting complex from photosynthetic bacteria. *Nature* **374**, 517–521.
21. Germeroth, L., Lottspeich, F., Robert, B. & Michel, H. (1993). Unexpected similarities of the B800–850 light-harvesting complex from *Rhodospirillum molischianum* to the B870 light-harvesting complexes from other purple photosynthetic bacteria. *Biochemistry* **32**, 5615–5621.
22. Hu, X., Xu, D., Hamer, K., Schulten, K., Koepke, J. & Michel, H. (1995). Predicting the structure of the light-harvesting complex II of *Rhodospirillum molischianum. Protein Sci.* **4**, 1670–1682.
23. Kleinekofort, W., Germeroth, L., van den Broek, J.A., Schubert, D. & Michel, H. (1992). The light-harvesting complex II (B800/850) from *Rhodospirillum molischianum* is an octamer. *Biochim. Biophys. Acta* **1140**, 102–104.
24. Germeroth, L. (1993). *Strukturelle Charakterisierung bakterieller Lichtsammelproteine*. [PhD thesis], Universität Frankfurt.
25. Timmins, P.A., Hauk, J., Wacker, T. & Welte, W. (1991). The influence of heptane-1,2,3-triol on the size and shape of LDAO micelles. *FEBS Lett.* **280**, 115–120.
26. Gast, P., Hemelrijk, P. & Hoff, A.J. (1994). Determination of the number of detergent molecules associated with the reaction centre from *Rhodopseudomonas viridis. FEBS Lett.* **337**, 39–42.
27. Kabsch, W. & Sander, C. (1983). Dictionary of protein secondary structure: pattern recognition of hydrogen-bonded and geometrical features. *Biopolymers* **22**, 2577–2637.
28. Jones, A., Zou, J.-Y., Cowan, S. & Kjeldgaard, M. (1991). Improved methods for building protein models in electron density maps and the location of error in these models. *Acta Cryst. A* **47**, 110–119.
29. Luzzati, V. (1952). Traitement statistique des erreurs dans la détermination des structures cristallines. *Acta Cryst.* **5**, 802–810.
30. Brünger, A.T. (1992). *X-PLOR, Version 3.1: a system for X-ray crystallography and NMR*. Yale University Press, New Haven, CT.
31. Brünger, A.T. (1992). Free R value: a novel statistical quantity for assessing the accuracy of crystal structures. *Nature* **335**, 472–474.
32. Brünger, A.T. (1993). Assessment of phase accuracy by cross validation: the free R value. Methods and applications. *Acta Cryst. D* **49**, 24–36.
33. Kleywegt, G.J. & Jones, T.A. (1996). Good model-building and refinement practice. *Methods Enzymol.*, in press.
34. Kleywegt, G.J., *et al.*, & Jones, T.A. (1994). Crystal structures of cellular retinoic acid binding proteins I and II in complex with all-trans-retinoic acid and a synthetic retinoid. *Structure* **2**, 1241–1258.
35. Fenna, R.E. & Matthews, B.W. (1975). Chlorophyll arrangement in a bacteriochlorophyll protein from *Chlorobium limicola. Nature* **258**, 573–577.
36. Matthews, B.W., Fenna, R.E., Bolognesi, M.C., Schmid, M.F. & Olson, J.M. (1979). Structure of a bacteriochlorophyll a-protein from the green photosynthetic bacterium *Prosthecochloris aestuarii. J. Mol. Biol.* **131**, 259–285.
37. Tronrud, D.E., Schmid, M.F. & Matthews, B.W. (1986). Structure and X-ray amino acid sequence of a bacteriochlorophyll-a protein from *Prosthecochloris aestuarii* refined at 1.9 Å resolution. *J. Mol. Biol.* **188**, 443–454.
38. Cogdell, R. & Frank, H. (1987). How carotenoids function in photosynthetic bacteria. *Biochim. Biophys. Acta* **895**, 63–79.
39. Nilsson, R., Merkel, P. & Kearns, D. (1972). Unambiguous evidence for the participation of singlet oxygen (1) in photodynamic oxidation of amino acids. *Photochem. Photobiol.* **16**, 117–124.
40. Anderson, P., Gillbro, T., Ferguson, L. & Cogdell, R. (1991). Absorption spectral shifts of carotenoids related to medium polarizability. *Photochem. Photobiol.* **54**, 353–360.
41. Zulauf, M. (1991). Detergent phenomena in membrane protein crystallization. In *Crystallization of Membrane Proteins*. (Michel, H., ed), pp. 53–72, CRC Press, Boca Raton, FL.
42. Roth, M., Lewit-Bentley, A., Michel, H., Deisenhofer, J., Huber, R. & Oesterhelt, D. (1989). Detergent structure in crystals of a bacterial photosynthetic reaction center. *Nature* **340**, 659–662.
43. Joo, T., Jia, Y., Yu, J.-Y., Jonas, D. & Fleming, G. (1996). Dynamics in isolated bacterial light harvesting antenna (LH2) of *Rhodobacter sphaeroides* at room temperature. *J. Chem. Phys.* **100**, 2399–2409.
44. Förster, T. (1948). Zwischenmolekulare Energiewanderung und Fluoreszenz. *Ann. Phys. NY* **2**, 55–75.
45. Gouterman, M. (1961). Spectra of porphyrins. *J. Mol. Spectrosc.* **6**, 138–163.
46. Weiss, C. (1972). The Pi electron structure and absorption spectra of chlorophylls in solution. *J. Mol. Spectrosc.* **44**, 37–80.
47. Visschers, R., Germeroth, L., Michel, H., Monshouwer, R. & van Grondelle, R. (1995). Spectroscopic properties of the light-harvesting complexes from *Rhodospirillum molischianum. Biochim. Biophys. Acta* **1230**, 147–154.
48. Eccles, J., Honig, B. & Schulten, K. (1988). Spectroscopic determinants in the reaction center of *Rhodopseudomonas viridis. Biophys. J.* **53**, 137–144.
49. Sakurai, J., (1994). *Modern Quantum Mechanics*. Addison & Wesley, NY.
50. Pearlstein, R. & Zuber, H. (1985). Exciton states and energy transfer in bacterial membranes: the role of pigment–protein cyclic unit structure. In *Antennas and Reaction Centers of Photosynthetic Bacteria*. (Michel-Beyerle, M., ed), pp. 53–61, Springer-Verlag, Berlin.
51. Novoderezhkin, V. & Razjivin, A. (1995). Exciton dynamics in circular aggregates: application to antenna of photosynthetic purple bacteria. *Biophys. J.* **68**, 1089–1100.
52. Hu, X., Xu, D., Hamer, K., Schulten, K., Koepke, J. & Michel, H. (1996). Prediction of the Structure of an Integral Membrane Protein – The Light-Harvesting Complex II of *Rhodospirillum molischianum*. In *Biological Membranes: A Molecular Perspective from Computation and Experiment*. (Merz, K. & Roux, B., eds, Birkhäuser, Cambridge, MA, in press.
53. Bylina, E., Robles, S. & Youvan, D. (1988). Directed mutations affecting the putative bacteriochlorophyll-binding sites in the light-harvesting I antenna of *Rhodobacter capsulatus. Isr. J. Chem.* **28**, 73–78.

54. Crielaard, W., Visschers, R., Fowler, G., van Grondelle, R., Hellingwerf, K., & Hunter, C. (1994). Probing the B800 bacteriochlorophyll binding site of the accessory light-harvesting complex from *Rhodobacter sphaeroides* using site-directed mutants. I. Mutagenesis, effects on binding, function and electrochromic behaviour of its carotenoids. *Biochim. Biophys. Acta* **1183**, 473–482.

55. Zuber, H. (1986). Structure of light-harvesting antenna complexes of photosynthetic bacteria, cyanobacteria and red algae. *Trends Biochem. Sci.* **11**, 414–419.

56. Schiffer, M., Chang, C.-H. & Stevens, F. J. (1992). The functions of tryptophan residues in membrane proteins. *Protein Eng.* **5**, 213–214.

57. van Grondelle, R. & Sundstrom, V. (1988). Excitation energy transfer in photosynthesis. In *Photosynthetic Light-Harvesting Systems.* (Scheer, H., ed), pp. 403–438, Walter de Gruyter & Co, Berlin, NY.

58. Otwinowski, Z. (1993). Oscillation Data Reduction Program. In *Proceedings of the CCP4 Study Weekend: Data Collection and Processing.* (Sawyer, L., Isaacs, N. & Bailey, S., eds), pp. 56–62, SERC Daresbury Laboratory, Warrington, UK.

59. Minor, W. (1993). *XDISPLAYF Program.* Purdue University.

60. Collaborative Computer Project No. 4. (1994). The CCP4 Suite: Programs for Protein Crystallography. *Acta Cryst. D* **50**, 760–763.

61. Sali, A. & Blundell, T.L. (1993). Comparative protein modelling by satisfaction of spatial restraints. *J. Mol. Biol.* **234**, 779–815.

62. Humphrey, W.F., Dalke, A. & Schulten, K. (1996). VMD – Visual Molecular Dynamics. *J. Mol. Graphics,* in press.

63. Nelson, M., *et al.,* & Kufrin, R. (1995). MDScope – A Visual Computing Environment for Structural Biology. *Comput. Phys. Commun.* **91**, 111–134.

64. Lattman, E. (1985). Diffraction methods for biological macromolecules. Use of the rotation and translation functions. *Methods Enzymol.* **115**, 55–77.

65. Rossmann, M., ed (1972). *The Molecular Replacement Method.* Gordon and Breach, NY.

66. Brünger, A.T. (1990). Extension of molecular replacement: a new search strategy based on Patterson correlation refinement. *Acta Cryst. A* **46**, 46–57.

67. Hauptman, H. (1982). On integrating the techniques of direct methods and isomorphous replacement. I. The theoretical basis. *Acta Cryst. A* **38**, 289–294.

68. Kleywegt, G.J. & Jones, A.T. (1994). Halloween... Masks and Bones. In *Proceedings of the CCP4 Study Weekend: From First Map to Final Model,* (Bailey, S., Hubbard, R. & Waller, D., eds), pp. 59–66, SERC Daresbury Laboratory, Warrington, UK.

69. Engh, R. & Huber, R. (1991). Accurate bond and angle parameters for X-ray protein structure refinement. *Acta Cryst. A* **47**, 392–400.

70. Lancaster, C.R.D. (1996). *The coupling of light-induced electron transfer to proton uptake in the photosynthetic reaction centre from* Rhodopseudomonas viridis. [PhD thesis], Universität Frankfurt.

71. Brooks, B.R., Bruccoleri, R.E., Olafson, B.D.J., van States, D., Swaminathan, S. & Karplus, M. (1983). CHARMm: a program for macromolecular energy, minimization, and dynamics calculations. *J. Comp. Chem.* **4**, 187–217.

72. Jones, T.A. (1992). a, yaap, asap, @#*? A set of averaging programs. In *Proceedings of the CCP4 Study Weekend: Molecular Replacement.* (Dodson, E.J., Glover, S. & Wolf, W., eds), pp. 92–105, SERC Daresbury Laboratory, Warrington, UK.

73. Germeroth, L., Reiländer, H. & Michel, H. (1996). Molecular cloning, DNA sequence and transcription analysis of the *Rhodospirillum molischianum* B800/850 light-harvesting genes. *Biochim. Biophys. Acta,* in press.

74. Altschul, S.F., Gish, W., Miller, W., Myers, E.W. & Lipman, D.J. (1990). Basic local alignment search tool. *J. Mol. Biol.* **215**, 403–410.